Hindawi
Journal of Advanced Transportation
Volume 2019, Article ID 9646091, 16 pages
https://doi.org/10.1155/2019/9646091

Research Article

Interlayer Working Conditions Classification and Treatment Measures of Airport Asphalt Pavement Overlay

Hongyu Ye,[1] **Xuancang Wang**,[1] **Naren Fang**,[1] **Ziyuan Su**,[2] **and Xiaowen Sun**[3]

[1]*School of Highway Engineering, Chang'an University, Xi'an 710064, China*
[2]*Henan Institute of Urban Planning and Design, Zhengzhou, Henan 450000, China*
[3]*CCCC FHDI Engineering Co., Ltd, Guangzhou 510230, China*

Correspondence should be addressed to Xuancang Wang; wxc2005@chd.edu.cn

Received 23 April 2019; Revised 17 October 2019; Accepted 25 October 2019; Published 31 December 2019

Academic Editor: Juan C. Cano

The bonding strength between the overlays of an airport asphalt pavement directly affects its service life. In this study, a finite element model of asphalt overlay on airport pavement of Juba Airport in South Sudan was established, and the elastic modulus of overlay, thickness of overlay, running state of aircraft, variation trend of interlayer shear stress under the action of load and temperature were obtained. The AHP-entropy method was used to calculate the combined weight of each influencing factor. The climate in hot and humid areas was further zoned, and a comprehensive classification of airport asphalt pavement overlay between hot and humid tropics was obtained. Four interlayer treatment measures (asphalt precoating, two oils and one aggregate, geotextile, and geogrid) and three interlayer materials (SBS-modified asphalt, ordinary hot asphalt, and SBS-modified emulsified asphalt) were designed and tested. Through shear test, wheel-load fatigue test, and pressurized seepage test, the variation trends of interlayer shear, crack resistance, and waterproofing under different combination schemes were obtained. Finally, the matching relationship between different working conditions and interlayer treatment measures was established. The results show that the actual working conditions of an airport asphalt pavement can be divided into three levels. Combined with the performance ranking of different materials and interlayer treatment measures, the recommended interlayer treatment measures for comprehensive classifications I, II, and III are two oils and one material + SBS-modified asphalt, asphalt precoating, or geogrid + SBS-modified emulsified asphalt or ordinary hot asphalt, and geotextile + ordinary hot asphalt, respectively. The working conditions in Juba Airport in South Sudan can be classified as comprehensive classification II, the recommended treatment measures for geogrid + ordinary hot asphalt.

1. Introduction

Airport pavements in hot and humid areas suffer from structural and functional deficiencies because of bad weather conditions, large number of aircrafts, and surge in air traffic [1, 2]. Asphalt pavement overlay can effectively improve the pavement performance and extend the pavement service life; this is widely used in airport pavement reinforcement [3, 4]. If the bond strength between the overlays is insufficient, harmful effects such as rutting, slippage, and congestion occur easily. According to the investigation, a large part of early pavement diseases is caused by poor interlayer bonding [4–6]. Therefore, interlayer treatment has become one of the key technical problems of airport asphalt pavement overlay.

Extensive studies have been conducted on the state of interlayer bonding. Kim et al. used coaxial and parallel direct shear tests to analyze the interlayer performance of asphalt pavement of existing expressway; complete continuity and discontinuity between layers were assumed to perform finite element analysis [7]. Chun et al. analyzed the effect of different interlayer bonding conditions on the pavement performance and service life using finite element method and full-scale test [6]. Zamora-Barraza et al. studied the interlayer properties of geotextiles, geogrids, and SAMI layers between the surface and base layers by dynamic tests [8]. Cleveland et al. designed a new test method to analyze the effect of different interlayer treatment measures on antireflective cracks and established a design equation between the fracture characteristics of geogrid and relaxation modulus characteristics of HMA [9]. Ferrotti et al. used geogrid + coating as the interlayer treatment for pavement structure; interlayer shear and four-point bending tests were carried out to evaluate the bonding properties of

asphalt layer [10]. Mai-Lan et al. performed a full-scale accelerated loading test to evaluate the effect of glass fiber geogrid at the bottom of asphalt layer on pavement fatigue life and interlayer performance [11]. Pasquini et al. evaluated the effect of glass fiber geogrid on interlayer performance through shear and bending tests [12]. Chen and Huang prepared three types of double-layer systems with dense porous asphalt concrete and asphalt macadam aggregate mixture; the bonding properties of bonding layer were measured by direct shear tests [13]. Yu et al. used a Hamburg Wheel Testing Machine to study the inhibiting effects of different types of stress-absorbing sandwiches such as SBS-modified asphalt sand concrete sandwich, asphalt rubber sand concrete sandwich, FRP–polyester pavement sandwich, and stress absorbing film on the development of reflective cracks [14]. In China, Fan studied the interlayer bonding properties, reflective crack resistance, and fatigue durability of three stress absorbing layers, namely, rubber asphalt stress absorbing layer, rubber powder modified asphalt mixture, glass grille + fiber modified asphalt mixture, between cement-stabilized base and surface layer by drawing test, APA test, and torsional shear fatigue test [15]. Wang et al. derived an indoor shear fatigue equation and developed a fatigue life prediction model by performing an indoor shear fatigue test of the bonding between cement-stabilized base and asphalt surface [5]. Li et al. established a finite element model of interlayer of base surface based on delamination failure theory and studied the effect of different interlayer treatment measures such as finish milling, rubber powder modified asphalt, SBS-modified asphalt, and matrix asphalt on the pavement performance by performing shear tests [16]. Zhang studied the continuity of permeable layer and synchronous gravel underlying seal to base and surface layer and evaluated the permeable oil penetration depth and shear strength of pavement structure [17]. Jia and Zhang evaluated the effect of rubber asphalt macadam seals on interlayer connectivity and proposed an index of interlayer connectivity effect to evaluate the implementation effect of rubber asphalt macadam seals and other interlayer treatment technologies [18].

Thus, many studies have been reported on interlayer treatment measures and crack resistance, but most of them focus on vehicle loads. Airplane loads are more complex than vehicle loads; interlayer mechanics of airport pavement is completely different from vehicle standard axle loads. Juba Airport in South Sudan is located in a hot and humid area with only one main runway. Climate factors and nonstop operation should be considered in interlayer treatment design. Therefore, domestic and foreign studies cannot be fully applied to Juba Airport. It is essential to evaluate the actual conditions of airport pavement in South Sudan and propose an interlayer treatment scheme suitable for different conditions of airport pavement in hot and humid areas.

In this study, a mechanical model was established for the pavement structure of South Sudan Airport in Africa. The effect of different factors on interlayer shear stress was analyzed. AHP-entropy method was used to determine the combined weight of each factor. Combined with the climate zoning in hot and humid areas, a comprehensive working condition classification of the Airport Asphalt Pavement overlay was obtained. Three types of interlayer materials and four types of interlayer treatment measures were tested by performing indoor shear test, wheel-load fatigue test, and pressurized seepage test. The performance and sequence of different treatment schemes were established. The treatment schemes under different working conditions were obtained. Finally, the actual working conditions of Juba Airport in South Sudan were determined, and the treatment measures for overlay were recommended.

2. Interlayer Mechanical Response of Airport Asphalt Pavement

2.1. Computing Model and Selection of Parameters

2.1.1. Selection of Pavement Structural Parameters. By investigating the pavement material and structure of Juba Airport in South Sudan, the parameters of pavement structure are shown in Table 1.

2.1.2. Load Action Parameters. Aircraft loads are mainly borne by the main undercarriage. Because of different structures of undercarriage of different aircraft types, compared with the vehicle load, the form of action on a road surface is more complex. The main models and wheel-load arrangement are shown in Figure 1.

After the asphalt overlay on the pavement of Juba Airport, the maximum aircraft type was upgraded from B737 to B767. According to the forecast data of air volume of Juba Airport, it is estimated that in 2020, B767 aircraft is the most demanding type of aircraft for the pavement of Juba Airport. In this study, B767-200 was used as the design aircraft [6, 19, 20]. The design parameters are shown in Table 2.

According to the specifications of asphalt pavement design of civil airports in China [21], an aircraft with the highest pavement requirement in design life was selected as the design aircraft. The single wheel load of main landing gear of aircraft was calculated as follows:

$$P_s = \frac{\rho \cdot G}{n_e n_w}, \tag{1}$$

where P_s is the single wheel load on main landing gear (kN), G is the designed maximum takeoff load (kN), ρ is the load distribution coefficient of main landing gear, n_e is number of main undercarriage, and n_w is number of wheels for single main undercarriage.

Single-wheel printing is usually set as an ellipse [22, 23] consisting of a rectangle and two semicircles. The length-to-width ratio of ellipse is 1 : 0.6. To facilitate the division of elements and to reduce the stress mutation around the elliptical load, the shape of load was simplified to a rectangle with a length-to-width ratio of 0.8712 : 0.6, as shown in Figure 2.

The length of ellipse was calculated using the following formula:

$$L = \sqrt{\frac{P_s \times 10^4}{5.227q}}, \tag{2}$$

Table 1: Structural parameters of airport pavement.

Pavement structure	Materials	Thickness (cm)	Resilience modulus (20°C, MPa)	Poisson ratio
Overlay asphalt pavement	SBS-modified asphalt concrete	10	1400	0.25
Overlay flexible base	Asphalt macadam	10	800	0.25
Original asphalt pavement	Asphalt concrete	10	600	0.25
Base	Graded broken stone	25	400	0.3
Subgrade	Compacted soil	-	40	0.4

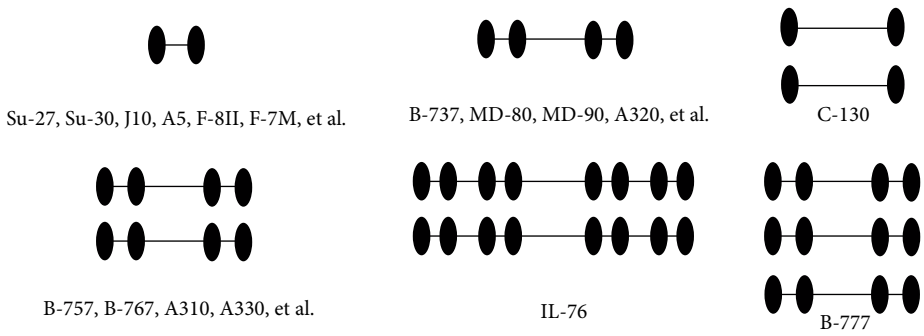

Figure 1: Common form of aircraft undercarriage.

Table 2: Design parameters of B767 aircraft.

Index	Parameters
Aircraft type	B767-200
Design maximum takeoff load (KN)	1343.50
Number of main undercarriage	2
Main landing gear spacing (m)	9.30
Load distribution coefficient of main landing gear	0.938
Main undercarriage type	Double axle and double wheel
Main landing gear tire pressure (MPa)	1.27

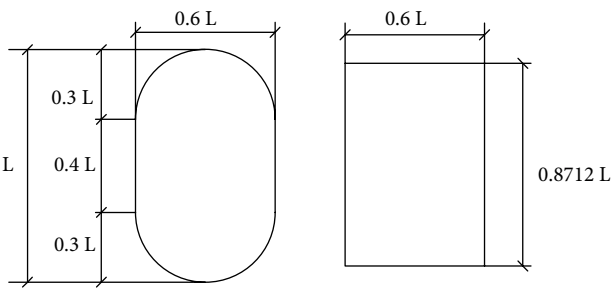

Figure 2: Single wheel load distribution of aircraft: (a) primary load distribution, (b) equivalent load distribution.

where L is the elliptical length (mm), and q is the main landing gear tire pressure (MPa).

According to formulas (1) and (2), the elliptical load was simplified as a rectangle with a wheel load of 0.4244 m × 0.2923 m; the tire grounding pressure is 1.27 MPa. The vehicle load of uniaxle and twin-wheel group proposed in Specifications for Design of Highway Asphalt Pavement is BZZ-100 [24]. The distribution form is shown in Figure 3.

2.1.3. Establishment of Finite Element Model. Because of the instantaneous action of wheel on the asphalt pavement of airport, the viscoplastic deformation of pavement structure is small. In mechanical calculations, the pavement layers are commonly assumed to be in full contact. However, because of construction level, external environment, and bonding materials, pavement layers are commonly not in complete contact. To simulate the actual pavement structure more truly, the contact state between the original asphalt pavement and flexible base is set as discontinuous, the friction coefficient is 0.7, and the rest is completely continuous [13–16, 22]. For convenience of calculation, it was assumed that the pavement is a multilayer elastic continuous system. And the boundary conditions were assumed as follows: The bottom is fixed, the left and right sides have no X-direction displacement, and the front and back sides have no Y-direction displacement. The model size is 5 m × 5 m × 5 m × 5 m, X is pavement longitudinal direction, Y is pavement transverse direction, and Z is depth direction. A finite element model was established by using an eight-node reduced integration element C3D8R [25, 26]. The pavement thickness and material parameters are shown in Table 1, and the load distribution is shown in Figure 3. The mesh density is 0.1 for the surface layer, 0.2 for the base layer, and 0.4 for the soil foundation. The location of area near the loading was encrypted to 0.05.

2.2. Influencing Factors of Interlayer Shear Stress on Pavement Overlay

2.2.1. Overlay Properties.

(1) Resilience Modulus of Overlay. To evaluate the effect of resilience modulus of overlay on interlayer shear stress, the modulus of overlay is maintained from 1000 MPa to 2000 MPa; the gradient is 200 MPa. Figure 4 shows the calculation results

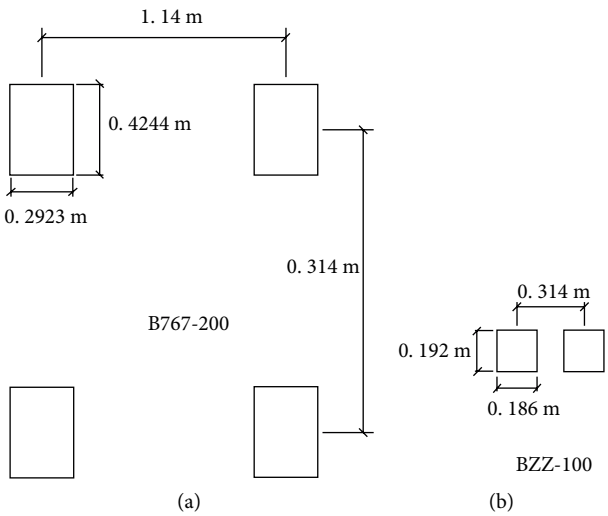

Figure 3: Load layout form: (a) B-767-200, (b) BZZ-100.

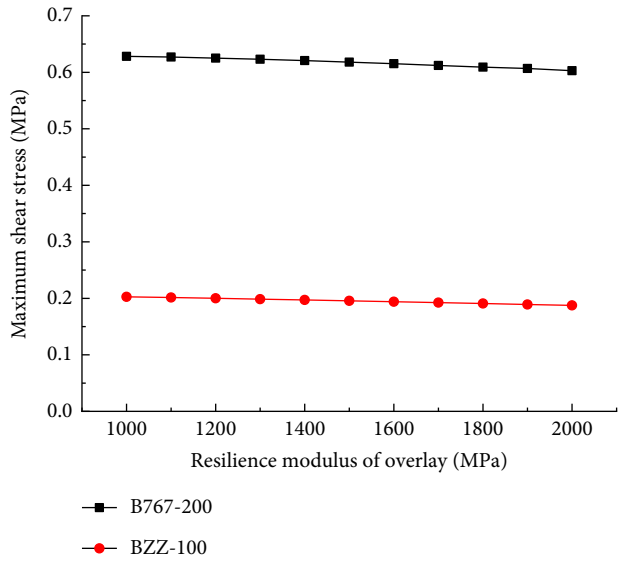

Figure 4: Effect of resilience modulus of overlay on maximum shear stress.

of maximum interlayer shear stress between B767-200 and BZZ-100.

Figure 4 shows that an increase in the resilience modulus of overlay asphalt concrete decreases the maximum interlayer shear stress, but it is not significant. When the modulus of overlay increases from 1000 MPa to 2000 MPa, the interlayer shear stress caused by B767-200 and BZZ-100 loads decreases by 4% and 6%, respectively.

(2) Overlay Thickness. The original asphalt pavement overlay thickness requirement is not less than 5 cm [21]; therefore, the design overlay thickness is 5–20 cm with a gradient of 2.5 cm increase. Figure 5 shows the relationship between maximum shear stress between overlays and thickness of overlays.

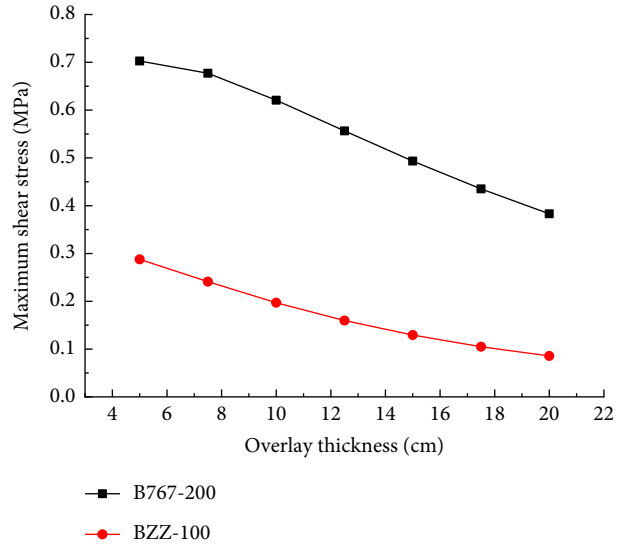

Figure 5: Effect of overlay thickness on maximum shear stress.

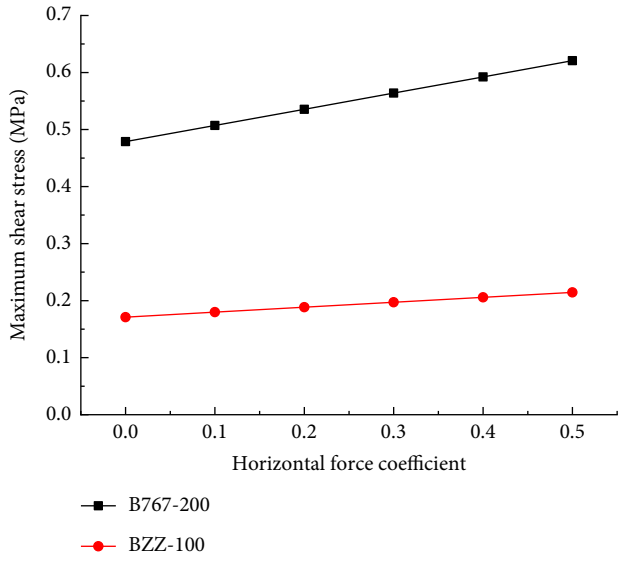

Figure 6: Effect of horizontal force coefficient on maximum shear stress of overlay.

Figure 5 shows that a change in overlay thickness significantly affects the interlayer shear stress. For B767-200, the shear stress decreased by 45.5% when the overlay thickness increases from 5 cm to 20 cm, whereas for BZZ-100, the maximum shear stress decreased by 70%. Therefore, an increase in overlay thickness significantly decreases the interlayer shear stress.

2.2.2. Interaction between Aircraft and Pavement.

(1) Horizontal Force Coefficient. The shear stress of overlay during acceleration, braking, or turning of aircraft is different from the normal driving state. Horizontal force coefficient was used to represent the different driving states of aircraft. The horizontal force coefficient f was selected as 0.1, 0.2, 0.3, 0.4,

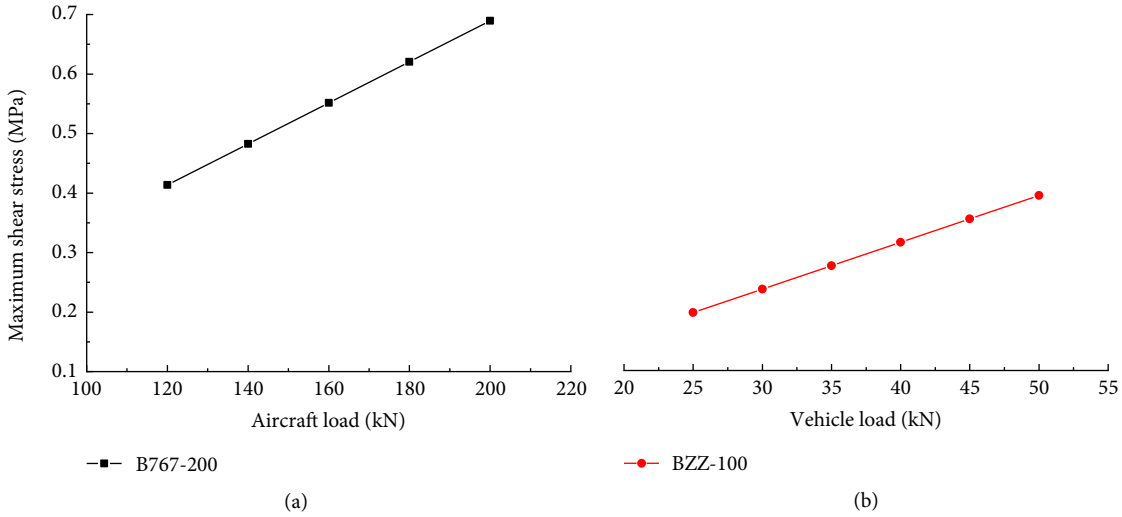

Figure 7: Effect of load on maximum shear stress of overlay: (a) B-767-200, (b) BZZ-100.

and 0.5. Figure 6 shows the calculated maximum shear stress of overlay on asphalt pavement.

Figure 6 shows that the horizontal force coefficient linearly increases, and the interlayer shear stress linearly increases. When the horizontal force coefficient increased from 0.1 to 0.5, the shear stress of B767-200 and BZZ-100 increased by 29.6% and 25.73% respectively, indicating that the shear stress of overlay during acceleration, braking, or turning is significantly higher than that of normal driving state.

(2) Load. The load range of B767-200 is much different from that of automobiles. The variation in interlayer shear stress under aircraft load and automobile load was compared. The wheel loads of aircraft were 120, 140, 160, 180, and 200 kN. The wheel loads of automobiles were 25, 30, 35, 40, 45, and 50 kN. Figure 7 shows the calculation results.

Figure 7(a) shows that the interlayer shear stress increases by 66.7% when the single wheel load increases from 120 KN to 200 KN. Figure 7(b) shows that the interlayer shear stress increases by 99.95% when the overload rate of vehicle load increases from 0% to 100%. Therefore, the load significantly affects the interlayer of pavement. If the load of aircraft take-off and landing on airport pavement is higher than the designed aircraft load, the interlayer is in a disadvantageous shear state.

2.2.3. External Environment. To simplify the calculation, it was assumed that the temperature of same pavement structure layer is the same. The effect of temperature on the resilience modulus E of asphalt mixture was characterized by BELLS-modified equation as follows [21, 27]:

$$E(T) = E_{20} \times 10^{\alpha(20-T)}, \quad (3)$$

where T is the temperature of asphalt mixture (°C); E_{20} is the resilient modulus of asphalt mixture at 20°C (MPa); α is the thermal sensitivity coefficient related to the mix ratio and thermodynamic properties of asphalt mixture; the range is 0.015–0.030.

Table 3: Resilience modulus of asphalt mixtures at different temperatures.

Materials	Resilience modulus (MPa)				
	20°C	30°C	40°C	50°C	60°C
SBS-modified asphalt concrete	1400	883	557	352	317
Asphalt macadam	600	600	600	600	600
Asphalt concrete	400	400	400	400	400
Graded broken stone	250	250	250	250	250
Compacted soil	740	40	40	40	40

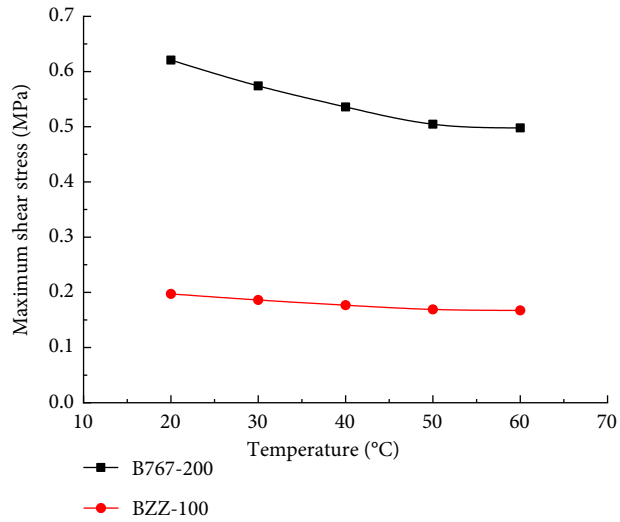

Figure 8: Effect of temperature on the maximum shear stress of overlay.

Using Formula (3), the resilience modulus of different structural layers at different temperatures was calculated, as shown in Table 3.

The variation in interlayer shear stress of asphalt pavement at different temperatures was calculated, as shown in Figure 8.

Figure 8 shows that for B767-200 and BZZ-100, the interlayer shear stress decreased by 19.77% and 17.16%, respectively, when the temperature increased from 20°C to 60°C. This shows that an increase of temperature decreases the shear stress of pavement to a certain extent. However, the shear strength decreases significantly at a high temperature; therefore, the lack of interlayer shear strength at a high temperature still leads to shear failure.

3. Interlayer Working Conditions of Airport Asphalt Pavement Overlays

3.1. Classification of Single Factor Working Conditions. Based on the mechanical analysis of different working conditions and pavement grading in specifications for asphalt pavement design of civil airports of China [21], the working conditions affecting the shear stress between overlays can be divided into three levels. It also evaluates each single-factor working condition grade (dimensionless), provides the basis for next comprehensive evaluation and determination of comprehensive working condition grading through the weight of each single factor, and obtains its specific assignment by the linear interpolation of single factor under the actual working condition. The assignment range is shown in Table 4.

3.2. AHP-Entropy Method for Calculating Comprehensive Weight. In this study, the AHP-entropy method was introduced to weigh both subjective and objective intentions. At the same time, the subjective weights of AHP method and the weights obtained from objective data were considered. The two methods were used to modify each other to determine the combined weights [22, 24]. The relationship can be expressed as follows:

$$\lambda_j = \frac{w_j v_j}{\sum_{j=1}^{m} w_j v_j} \quad (j = 1, 2, \ldots, m), \tag{4}$$

where w_j is the subjective weight determined by AHP method; v_j is the objective weight determined by the entropy method; λ_j is the optimal combination weight.

By combining the weights of AHP and entropy methods, the comprehensive working conditions weights of influencing factors of interlayer shear stress on airport pavement were obtained, as shown in Table 5.

According to the combined weight, the influence model of each working condition on the shear stress between the overlays of airport asphalt pavement can be obtained as follows:

$$I_0 = 0.2501I_h + 0.0184I_e + 0.1012I_\mu + 0.5426I_G + 0.0877I_t, \tag{5}$$

where I_0 is comprehensive working condition evaluation number; I_h, I_e, I_μ, I_G, and I_t are the dimensionless evaluation numbers of overlay thickness, resilience modulus, horizontal force coefficient, load, and temperature, respectively.

The climate and environment in humid and hot regions of Africa are more complex. In this study, the climate zoning in hot and humid areas was considered separately. To avoid repeated calculation and remove the evaluation index of temperature, the influence model can be simplified as follows:

$$I_0 = 0.2741I_h + 0.0203I_e + 0.1109I_\mu + 0.5947I_G. \tag{6}$$

According to the formula of comprehensive working condition evaluation number, the single-factor assignment in Table 4 was substituted into the comprehensive working condition evaluation index model, and the dimensionless evaluation number was obtained according to the calculation. Regardless of external environment impact, the combined working conditions of airport pavement overlay can be divided into three levels, and the classification is shown in Table 6.

Table 4: Classification of single-factor working condition of overlay.

Single factor working condition grade	I	II	III
Assignment	0–33	33–67	67–100
Overlay thickness (cm)	5–7	8–15	15–20
Modulus of overlay (MPa)	800–1000	1000–1500	1500–2000
Horizontal force coefficient	0.3–0.5	0.2–0.3	0–0.2
Single wheel load of main landing gear at maximum take-off weight (kN)	200–300	100–200	50–100

3.3. Climate Zoning in Hot and Humid Areas. The results of Section 2.2.3 show that temperature significantly affects the interlayer shear stress of overlay on airport pavement. At the same time, the overlay in hot and humid areas should also exhibit good waterproof performance. According to the analysis mentioned above, the hottest monthly average temperature, annual average rainfall, and diurnal average temperature difference were selected as three indicators for the climate zoning of airport pavement overlay in hot and humid areas. Combined with the climate and rainfall conditions, a three-level climate zoning is proposed, as shown in Table 7.

According to the three indicators mentioned above and considering the convenience of practical applications, the climate zoning of airport overlay in hot and humid areas can be divided into three levels. In the classification, I and II are the main divisions; III is the supplementary division, as shown in Table 8.

3.4. Comprehensive Classification of Interlayer Working Conditions. Based on the results of climatic zoning in humid and hot regions in Table 8 and the revision of temperature increase shown in Table 6, a classification of comprehensive working conditions of asphalt pavement overlay in airports in humid and hot tropical regions is proposed. It can be divided into three levels: poor working conditions in Grade I, general working conditions in Grade II, and good working conditions in Grade III. The classification results are shown in Table 9.

Table 5: Optimal weight determined by AHP-entropy method.

Working condition	Weight of AHP method (subjective weight)	Weights of entropy method (objective weight)	Combination weight of AHP-entropy method (optimizing weight)
Overlay thickness	0.2376	0.2571	0.2501
Resilience modulus of overlay	0.0594	0.0756	0.0184
Horizontal force coefficient	0.1079	0.2291	0.1012
Load	0.4317	0.3070	0.5426
Temperature	0.1634	0.1311	0.0877

Table 6: Classification of airport asphalt pavement overlay combination working condition (regardless of external environment impact).

Working condition classification[1]	1	2	3
Evaluation number	0–33	34–66	67–100

[1]The flexible layer between pavement and old road can reduce the working condition by one level.

Table 7: Three-stage climate zoning of airport overlay in hot and humid area.

Level 1 zoning	Ultrahigh temperature area	High temperature area
Hottest monthly mean temperature (°C)	≥40	<40
Region of origin	Hot and humid northern tropical desert climate area	Tropical rainforest climate zone and tropical grassland climate zone
Level 2 zoning	Rainy area	Less rainfall area
Average annual rainfall (mm)	≥1000	<1000
Region of origin	Tropical rainforest climate area near the equator	Other regions except tropical rainforest climate zone
Level 3 zoning	Regions with large temperature difference	Regions with small temperature difference
Average temperature difference between day and night (°C)	≥15	<15
Region of origin	Hot and humid northern tropical desert areas	Areas other than tropical desert climatic areas

Table 8: Comprehensive climate zoning of airport overlay in hot and humid area.

Working condition classification	I	II	III
Climatic zoning	Tropical desert climate and tropical rainforest climate area	Tropical steppe climate zone	Other areas
Actual working condition	High temperature and rainy year-round or less precipitation year-round, but a large temperature difference	Year-round high temperature, divided into dry and wet seasons	Small temperature difference, less rainfall and moderate temperature

Table 9: Comprehensive classification of airport asphalt pavement overlay.

Comprehensive classification	Climate I area	Climate II area	Climate III area
Working condition 1	I	I	II
Working condition 2	I	II	II
Working condition 3	II	II	III

4. Performance of Airport Pavement Overlay under Different Materials and Interlayer Treatment Measures

In this study, three types of interlayer materials were used: ordinary hot asphalt, SBS-modified asphalt, and SBS-modified emulsified asphalt. Four types of interlayer treatment measures were used: asphalt precoating, two oils and one aggregate distributed stress absorbing layer, geotextile, and geogrid. The 12 combination schemes mentioned above were tested by indoor shear test, wheel-load fatigue test, pressurized seepage test, and high-temperature rutting test.

Among them, two oils and one aggregate is a new interlayer treatment measure, i.e., lower asphalt and intermediate

Table 10: Technical specifications of asphalt.

Technical indicators			Unit	Measured value	Standard [20]
Ordinary asphalt	Penetration (25°C, 100 g, 5 s)		0.1 mm	43	40–120
	Softening point TR&B		°C	84.0	≥80
	Dynamic viscosity (135°C)		Pa·s	1.64	≤3
	Elastic recovery (25°C)		%	29126	≥20000
	RTFOT residue	Quality loss	%	0.14	≤0.6
		Penetration ratio 25°C	%	71	≥65
	Density (15°C)		g/cm^3	0.986	–
SBS-modified asphalt	Penetration (25°C, 100 g, 5 s)		0.1 mm	67.2	60–80
	Ductility (5°C, 5 cm/min)		cm	44.8	≥30
	Softening point TR&B		°C	79.0	≥55
	Dynamic viscosity (135°C)		Pa·s	1.19	≤3
	Elastic recovery (25°C)		%	88	≥65
	Density (15°C)		g/cm^3	1.016	–
	RTFOT residue	Quality loss	%	−0.4	≤±1
		Penetration ratio 25°C	%	65	≥60
		Ductility 5°C, 5 cm/min	cm	31	≥20
SBS-modified emulsified asphalt	Weight of screen residue (1.18 mm), ≤		%	0.02	0.1
	ductility (5°C, 5 cm/min)		cm	44.8	≥30
	Storage stability	1 d, ≤	%	0.5	1
		5 d, ≤	%	1.2	5
	Evaporated residue	Content, ≤	%	52	50
		Penetration (25°C, 100 g, 5 s)	0.1 mm	59	40–120
		Softening point, ≤	°C	53.5	50
		Ductility (5°C), ≥	0.1 mm	35	20
		Solubility (TCE), ≥	°C	98.3	97.5
	Viscosity	EngLa viscosity E25	—	7	1–10
		Asphalt standard viscosity C25,3	S	15	8–25

crushed stones are first sprayed on the old pavement in sequence, and the top asphalt is covered on crushed stones, significantly improving the asphalt coverage of crushed stones, increasing the interlayer bonding between the old and new pavements, and effectively acting as the stress absorption layer.

4.1. Technical Properties of Raw Materials

4.1.1. Asphalt. The main technical indexes of ordinary hot asphalt, SBS-modified asphalt, and SBS-modified emulsified asphalt are shown in Table 10.

4.1.2. Design of Asphalt Materials. The aggregate gradation of AC-13 and AC-20 is shown in Figure 9.

According to the results of Marshall test, the optimum asphalt contents of AC-13 and AC-20 of asphalt materials are shown in Table 11.

4.2. Determination of Optimum Amount of Three Interlayer Asphalt Materials. To simulate the actual construction situation of solid project, the steps of "laying a lower asphalt layer—setting stress absorption layer—laying upper asphalt layer" were used to make the cylinder specimen of stress absorption layer with a diameter of φ 10 cm × 10 cm. The

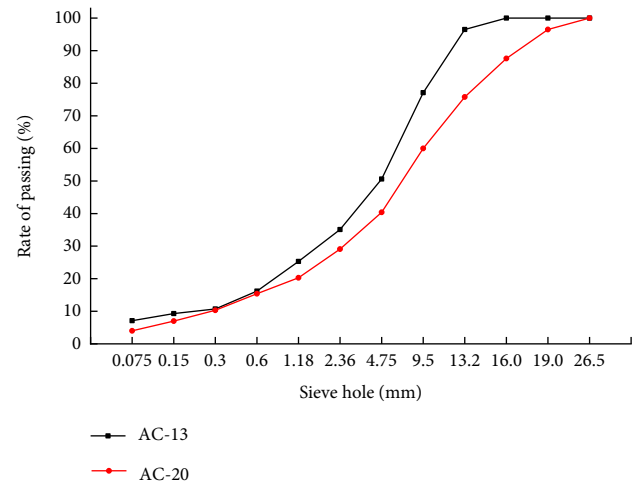

Figure 9: Aggregate gradation.

Table 11: Optimum asphalt content.

Type of mixture	Optimum asphalt content (%)
AC-13	4.6
AC-20	4.0

(a) (b) (c) (d)

Figure 10: Preparation of specimens (a) asphalt precoating, (b) two oils and one aggregate, (c) the used geotextile, (d) the used glass fiber geogrid.

(a) (b) (c)

Figure 11: Interlayer shear test: (a) formed double-layer rutting plate, (b) core drilling sampling, (c) shear test.

properties of asphalt materials are shown in Table 10. The steps can be described as follows:

(1) A rutting slab of AC-20 asphalt mixture with 30 cm × 30 cm × 5 cm was used to simulate the underlying structure of pavement.

(2) After forming the lower rutting plate, the following four schemes were carried out for interlayer treatment.

(a) Interlayer asphalt material is evenly distributed on the surface of AC-20 rutting plate. SBS-modified asphalt, ordinary hot asphalt, and SBS-modified emulsified asphalt were sprayed on the surface of specimens. The quantity of asphalt spreading is 0.6, 0.9, 1.2, 1.5, and 1.8 kg/m^2. Then, the gravel material with a particle size of 10–15 mm was evenly distributed and compacted. The spraying amount of precoating gravel was 6, 7, 8, and 9 kg/m^2, respectively. The test temperature was 25°C. The specimen is shown in Figure 10(a).

(b) A crushed stone with a particle size of 10–15 mm was selected as the raw material for two oils and one aggregate. The optimum amount of crushed stone was determined by asphalt precoating test. The interlayer asphalt material was evenly distributed on the surface of AC-20 rutting board, and then the gravel was distributed and compacted. Finally, the same interlayer material was distributed on the surface of gravel. Three interlayer materials were smeared separately for comparison. The spraying amount of lower asphalt was 0.6, 0.9, 1.2, 1.5, and 1.8 kg/m^2. The spraying amount of upper asphalt was 0.2, 0.3, 0.4, 0.5, and 0.6 kg/m^2. The test temperature was 25°C. The specimen is shown in Figure 10(b).

(c) Different interlayer asphalt materials were sprayed on the surface of AC-20 rutting plate. Then, the geotextile cut to 300 × 300 mm was evenly laid on the surface of specimens and rolled, as shown in Figure 10(c). The spraying amount of materials was 0.4, 0.6, 0.8, 1.0, and 1.2 kg/m^2. The test temperatures were 25, 40, and 60°C.

(d) Different interlayer asphalt materials were sprayed on the surface of AC-20 rutting board; then, a glass fiber geogrid cut to 300 × 300 mm was laid on the surface of specimens and rolled as shown in Figure 10(d). The spraying amount of materials was 0.4, 0.6, 0.8, 1.0, and 1.2 kg/m^2. The test temperatures were 25, 40, and 60°C.

(3) The specimens after interlayer treatment were placed in a 30 cm × 30 cm × 10 cm test model; AC-13 asphalt mixture was added. After rolling the specimens, a double-layer rutting plate was formed. Core samples of φ 10 cm × 10 cm were drilled on the formed double-layer composite rutting plate. Shear tests were carried out on the core samples using a shear tester [28, 29]; the shear rate was 10 mm/min. The shear test is shown in Figure 11.

Figure 12 shows the shear test results of specimens with precoated interlayer treatments.

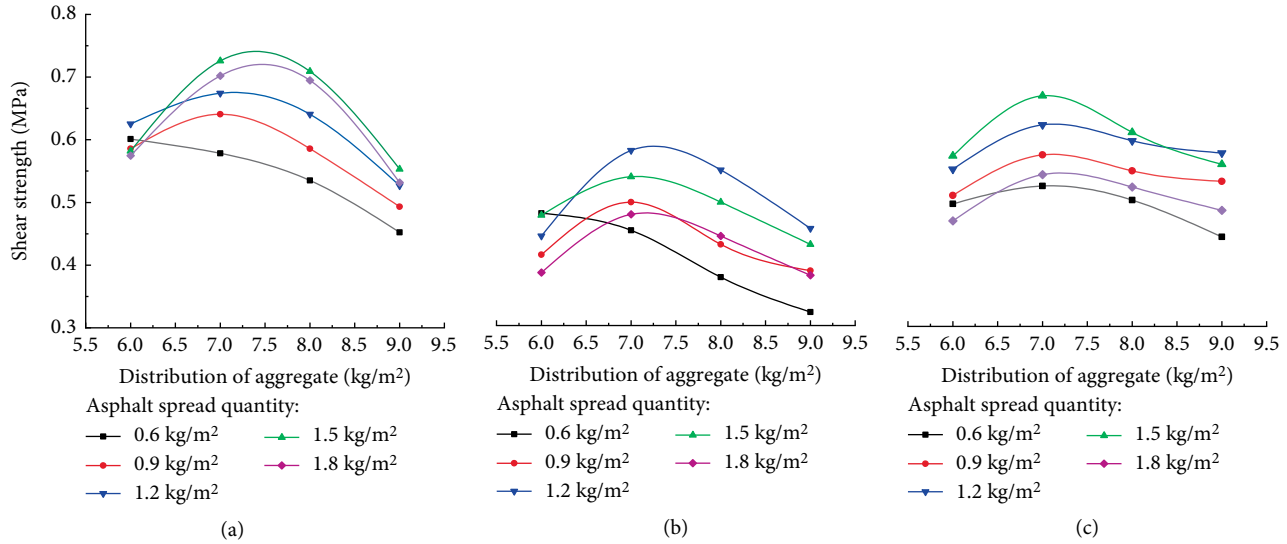

FIGURE 12: Shear strength of specimens with precoated interlayer treatment: (a) SBS-modified asphalt, (b) SBS-modified emulsified asphalt, (c) ordinary hot asphalt.

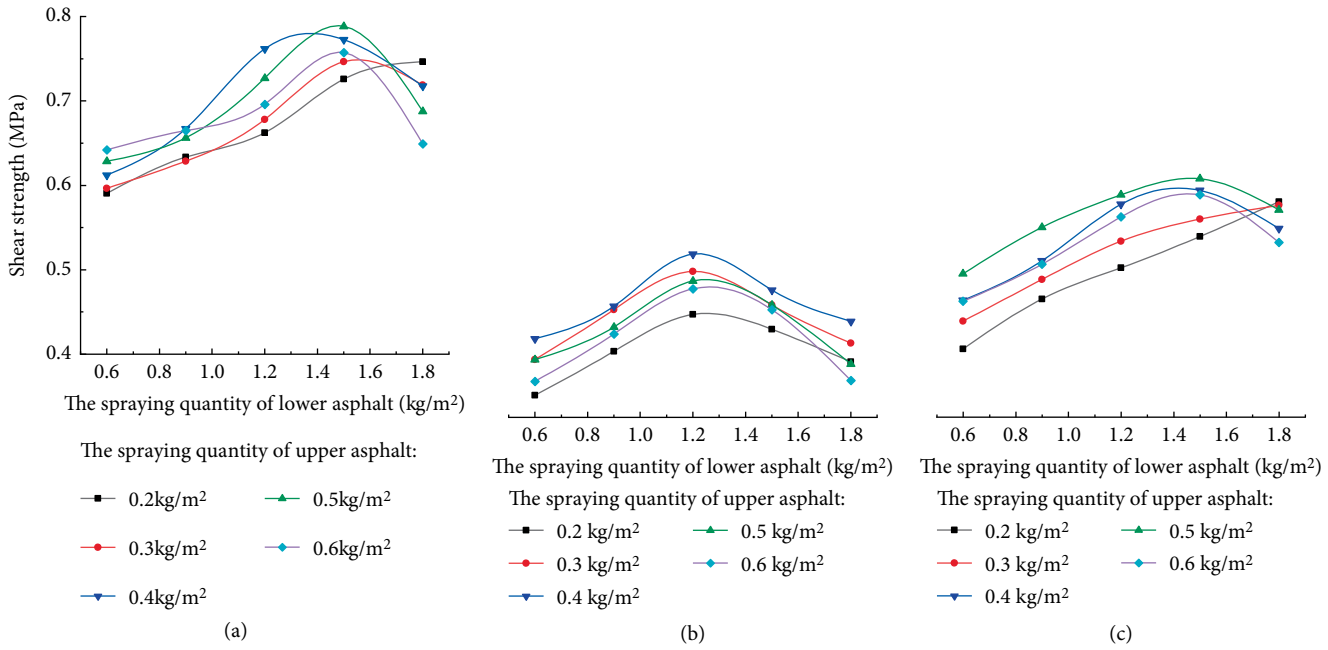

FIGURE 13: Shear strength of specimens with two oils and one aggregate interlayer treatment: (a) SBS-modified asphalt, (b) ordinary hot asphalt, (c) SBS-modified emulsified asphalt.

Figure 12 shows that when the interlayer treatment measure is precoated, the optimum asphalt spraying amounts of SBS-modified asphalt, ordinary hot asphalt, and SBS-modified emulsified asphalt are 1.5, 1.2, and 1.5 kg/m^2 respectively, and the optimum amount of aggregate is 7 kg/m^2. Therefore, the interlayer treatment scheme of "two oils and one aggregate" used an amount of 7 kg/m^2 gravel to prepare specimens for shear test. The results are shown in Figure 13.

Figure 13 shows that when the interlayer treatment measure is two oils and one aggregate, the optimum spraying amount of lower asphalt of SBS-modified asphalt, ordinary hot asphalt, and SBS-modified emulsified asphalt are 1.5, 1.2, and 1.5 kg/m^2, respectively. The optimum spraying amount of upper asphalt of SBS-modified asphalt, ordinary hot asphalt, and SBS-modified emulsified asphalt are 0.5, 0.4, and 0.5 kg/m^2, respectively. The shear test results of specimens with geotextile interlayer treatments are shown in Figure 14.

Figure 14 shows that when the interlayer treatment measure is geotextiles, the optimum spraying amount of SBS-modified asphalt, ordinary hot asphalt, and SBS-modified emulsified asphalt are 1.0, 0.8, and 1.0 kg/m^2, respectively. The shear test results of specimens with geogrids interlayer treatments are shown in Figure 15.

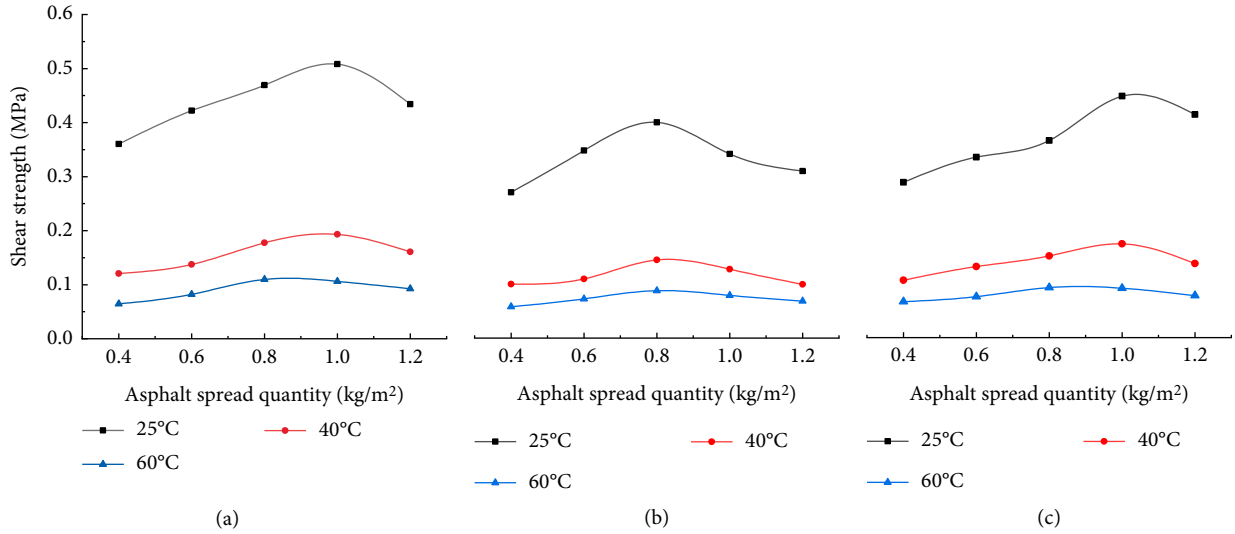

Figure 14: Shear strength of specimens with geotextiles interlayer treatment: (a) SBS-modified asphalt, (b) ordinary hot asphalt, (c) SBS-modified emulsified asphalt.

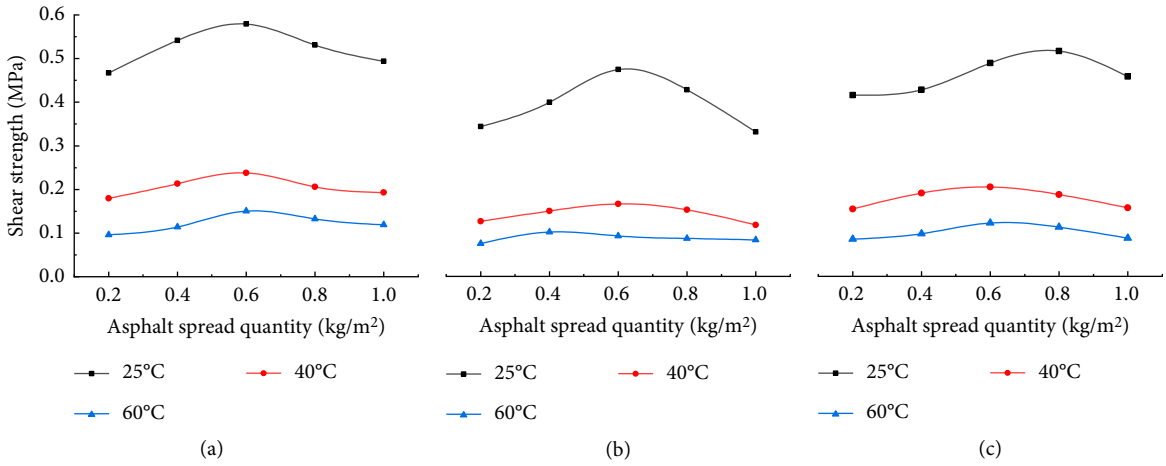

Figure 15: Shear strength of specimens with geogrids interlayer treatment: (a) SBS-modified asphalt, (b) ordinary hot asphalt, (c) SBS-modified emulsified asphalt.

From Figure 15, the optimum asphalt content for different interlayer materials can be obtained, as shown in Table 12.

4.3. Test Scheme

(1) Shear Test. Shear tests were carried out following the test method described in Section 4.2. The test temperatures were set as 25, 30, 40, 50, and 60°C.

(2) Wheel-Load Fatigue Test. A double-layer rutting board made of 4.2 sections was cut into 30 cm × 10 cm × 10 cm trabecular specimens. A 20-cm rubber layer was padded on the bottom of beam specimen before loading, as shown in Figure 16. The test temperature was 25°C. The trabecular specimens were placed in a rutting tester under repeated wheel loads of standard test with a wheel pressure of $p = 0.7$ MPa. Loading period T is 1.43 s. The development of structural cracks in different interlayer treatment schemes was observed; the number of wheel loads was recorded.

Table 12: Optimum spraying amount for interlayer treatment of geogrids.

Interlayer material	Temperature (°C)		
	25°C	40°C	60°C
SBS-modified asphalt	0.6	0.6	0.6
Ordinary hot asphalt	0.6	0.6	0.4
SBS-modified emulsified asphalt	0.6	0.8	0.8

(3) Pressurized Seepage Test. According to the material and method described in Section 3.2, double-layer rutting plate specimens were obtained. A pressure seepage tester [29, 30] was used to pressurize different interlayer materials. The water pressure was 0.55 MPa. The beginning time of seepage and time of severe seepage were recorded.

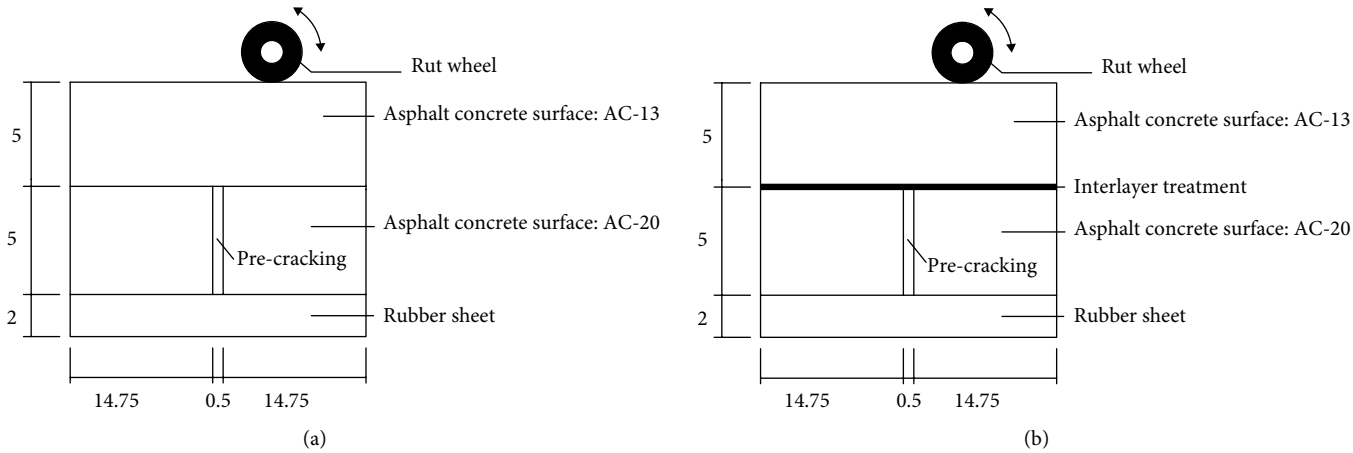

Figure 16: Wheel-load fatigue test model: (a) no interlayer treatment, (b) different interlayer materials and treatment measures.

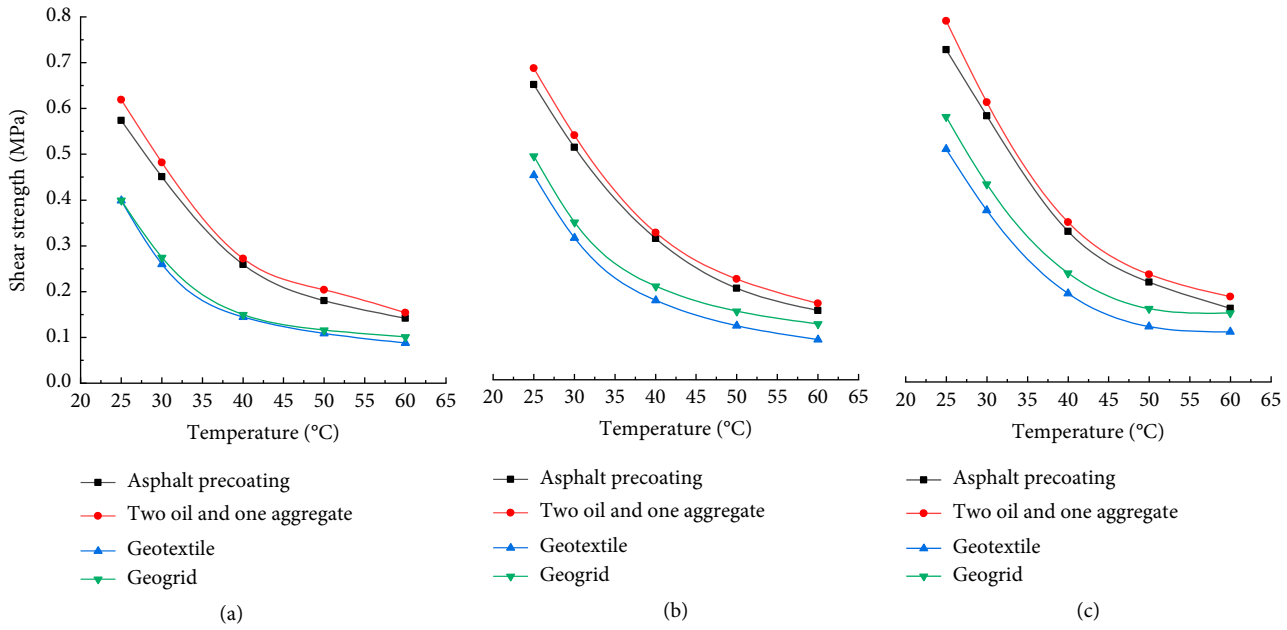

Figure 17: Comparison of shear resistance between different materials and different layers: (a) ordinary hot asphalt, (b) SBS-modified asphalt, (c) SBS-modified emulsified asphalt.

4.4. Test Results and Analysis

4.4.1. Interlayer Shear Resistance of Overlay. Figure 17 shows the shear properties obtained from interlayer shear tests.

Figure 17 shows that:

(1) Among the four interlayer treatment measures, the shear strength of specimens treated with two oils and one aggregate interlayer treatment is the highest. Taking the ordinary hot asphalt interlayer material as an example, compared with two oils and one aggregate interlayer treatment, the shear strength of specimens treated with precoated asphalt interlayer treatment decreased by 6.68%, 6.12%, and 9.29% at 25, 40, and 60°C, respectively. The shear strength of specimens treated with geotextile interlayer treatment is found to be the lowest. This decreased by 41.91%, 41.6%, and 40.54% at 25, 40, and 60°C, respectively. The shear strength of specimens treated with geogrid interlayer treatment decreased by 38.25%, 30.35%, and 25.99% at 25, 40, and 60%, respectively.

(2) Among the three interlayer materials, the shear strength of specimens treated with SBS-modified asphalt was the highest. Taking two oils and one aggregate interlayer treatment as an example, compared with SBS-modified asphalt interlayer material, the shear strength of specimens treated with ordinary hot asphalt interlayer material was the lowest. This decreased by 21.45%, 22.06%, and 17.74% at 25, 40, and 60°C, respectively. Furthermore, the shear strength of specimens treated with SBS-modified emulsified asphalt interlayer material decreased by 13.71%, 8.02%, and 10.75% at 25, 40, and 60°C, respectively.

(3) The effect of temperature on the shear strength of specimens is very significant. Taking the precoated asphalt

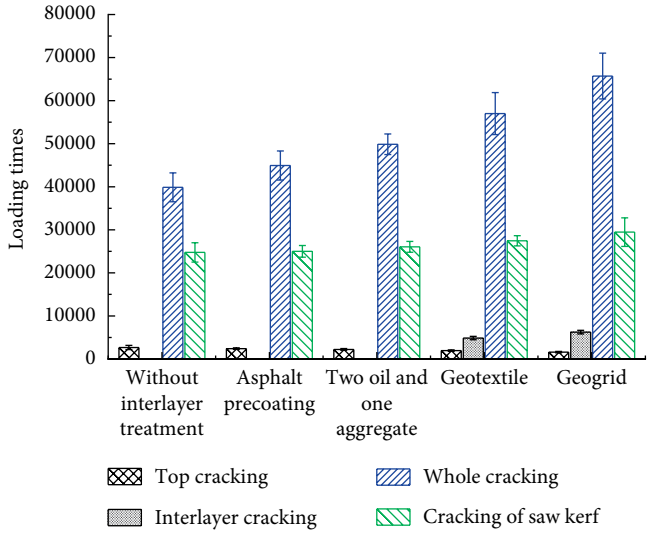

Figure 18: Comparison of treatment load fatigue test results between different layers.

interlayer treatment as an example, when the temperature increased from 25°C to 40°C, the shear strength of specimens using SBS-modified asphalt, ordinary hot asphalt, and SBS-modified emulsified asphalt as the interlayer materials decreased by 54.7%, 54.8%, and 52.1%, respectively. When the temperature increased from 25°C to 60°C, the shear strength of specimens using the three interlayer materials decreased by 77.8%, 75.3%, and 76.5%, respectively. The shear stress variation trend of specimens with two oils and one aggregate interlayer measures is consistent with this trend. When the interlayer treatment is geotextile, the shear strength of different materials at 25°C is ~3 and 5 times of that at 40°C and 60°C, respectively. When the interlayer treatment is geogrid, the trend becomes 2 and 4 times, respectively. In conclusion, the shear resistance of interlayer materials is insufficient under unfavorable high temperature conditions. Interlayer treatment measures and interlayer materials with a high shear strength should be selected in a high-temperature area.

4.4.2. Crack Resistance of Overlay. Figure 18 shows the test results of crack resistance between overlays.

Figure 18 shows that the top cracks occurred when the specimen was loaded 1500–3000 times. The fastest crack on the top is observed for the specimen treated with a geogrid interlayer treatment. For the specimens treated with geotextiles and grilles, interlayer cracking occurs after 6000–6500 times. This phenomenon did not occur in the specimens treated with two oils and one material, precoated interlayer treatment, and without interlayer treatment. This is because of the reduction of bonding between geotextiles, geogrids, and asphalt layer by the repeated action of wheel loads. Then, the crack propagates slowly until the crack appears at the saw kerf of specimen loaded 20,000–30,000 times. At 40,000–60,000 times, the entire specimen was destroyed. Because the stress-absorbing layer can diffuse the load above the layer along the horizontal direction, the crack resistance of entire structure increased. When whole cracking or the cracking of saw kerf is used as the evaluation criteria for crack resistance, Geogrid is the best interlayer treatment measure for ranking anticrack performance. The crack resistance of specimens without interlayer treatment is the worst.

Table 13: Test results of pressure seepage between different layers.

Treatment measures	Waterproof material	Beginning seepage time (s)	Starting time of severe seepage (s)
Asphalt precoating	Ordinary hot asphalt	203	375
	SBS-modified emulsified asphalt	413	494
	SBS-modified asphalt	389	463
Two oils and one aggregate	Ordinary hot asphalt	342	435
	SBS-modified emulsified asphalt	437	563
	SBS-modified asphalt	399	521
Geotextile	Ordinary hot asphalt	>600[1]	>600[1]
	SBS-modified emulsified asphalt	>600[1]	>600[1]
	SBS-modified asphalt	>600[1]	>600[1]
Geogrid	Ordinary hot asphalt	64	102
	SBS-modified emulsified asphalt	131	149
	SBS-modified asphalt	112	165

[1]The test is based on 600 seconds and no longer counts for more than 600 seconds.

4.4.3. Antiseepage Performance of Overlay. Table 13 shows the test results of antiseepage property between overlays.

Table 13 shows that modified emulsified asphalt exhibits the best waterproof performance; the worst performance is exhibited by ordinary hot asphalt. This is related to the uniformity and thickness of film formation of viscous oil materials. Modified emulsification is a liquid at room temperature and has good fluidity. It is easy to form a uniform thick film when it is sprayed. Therefore, the waterproof performance of modified emulsification is still better after the stabbing of hot aggregate. However, ordinary hot asphalt and SBS-modified asphalt should be heated to a liquid. The uniformity and thickness of film are the key factors for the waterproof performance of adhesive materials. Therefore, when spraying an adhesive material in construction, the spraying should be uniform. To satisfy the interlayer shear strength, the amount of adhesive material should be increased as much as possible to achieve good waterproof performance.

Table 14: Comprehensive properties of interlayer materials.

Interlayer materials	Construction requirements	Whether need to stop sailing	Shear strength	Antiseepage performance	Classification of material properties
SBS-modified emulsified asphalt	Emulsified asphalt distributer	Yes	Middle	Good	2
Ordinary hot asphalt	Intelligent asphalt distributer	No	Poor	Poor	1
SBS-modified asphalt	Intelligent asphalt distributer	No	Good	Middle	3

The best waterproof performance of different interlayer treatments was achieved using geotextile, because a layer of waterproof film is formed after the geotextile is soaked with asphalt to prevent water from entering the lower layer of specimen. It was found that seepage occurs around the upper layer of geotextile specimen. The experimental group of asphalt precoating and geogrid showed seepage at the lower part of specimen. The waterproof performance of absorbing layer is lower than that of geotextile; it is fragmented. The pores in stone cannot completely prevent the flow of water, and the grille itself has no waterproof performance. It entirely relies on the asphalt sprayed before the grille to prevent water penetration; therefore, its antiseepage performance is the worst. The waterproof performance of synchronous crushed stone with "two oils and one material" is slightly better than that of asphalt precoating, because the film thickness of "two oils and one material" is slightly larger.

5. Matching Relationship between Working Conditions and Treatment Schemes of Airport Pavement Overlay

5.1. Performance Classification of Interlayer Materials. By analyzing the shear and seepage test results of SBS-modified emulsified asphalt, ordinary hot asphalt, and SBS-modified asphalt, a comprehensive ranking of properties of various materials was obtained, as shown in Table 14. According to the material properties of interlayer, considering the shear strength, impermeability, and whether sailing should be stopped, the interlayer materials can be divided into three levels with the best performance at level 1 and the worst performance at level 3.

5.2. Performance Classification of Interlayer Treatment Types. According to the test results shown in Section 3.4, shear strength is the main factor; crack resistance and impermeability were considered. Different types of interlayer treatment can be divided into three levels. The first level treatment has the best effect; the third level treatment has the worst effect. The specific classification is shown in Table 15.

5.3. Matching Relationship between Actual Working Conditions and Treatment Schemes. According to the classification of comprehensive working conditions, the interlayer treatment schemes under different working conditions are finally proposed by combined performance comparison of interlayer materials and treatment measures, as shown in Table 16.

Table 15: Single performance classification of interlayer treatment scheme.

Classification of treatment measures	Interlayer treatment measures
1	Two oils and one aggregate
2	Asphalt precoating or geogrid
3	Geotextile

Table 16: Grading treatment scheme under different comprehensive working conditions.

Comprehensive classification	Interlayer treatment measures	Interlayer materials[1]
I	Two oils and one aggregate	SBS-modified asphalt
II	Asphalt precoating or geogrid	SBS-modified emulsified asphalt or ordinary hot asphalt
III	Geotextile	Ordinary hot asphalt

[1]Modified emulsified asphalt was not used when sailing cannot stop.

5.4. Engineering Verification in Juba Airport in South Sudan. Based on the analysis mentioned above, taking the Juba Airport in South Sudan as an example, comprehensive classification and interlayer materials and treatment measures of the overlay are determined, and on-site observation is carried out.

The pavement structure of Juba Airport in South Sudan has a 5 + 6 + 7 cm asphalt overlay +10 cm flexible base + original pavement structure; the overlay thickness is 18 cm. The resilience modulus of overlay is 1400 MPa. Juba airport in South Sudan is in a high temperature and rainy environment, which is not conducive to braking. The horizontal force coefficient is taken as 0.5. As shown in Table 2 and Formula (1) of Section 2.1.2, the single wheel load of main landing gear with the maximum takeoff weight of designed aircraft is 157.53 kN. As shown in Table 4, the linear interpolation method is used to calculate the single-factor values shown in Table 17.

Using Formula (4), the comprehensive working condition evaluation index was found to be 61.35. Table 6 shows that

Table 17: Single-factor values of Juba airport in South Sudan.

Factors	Overlay thickness (cm)	Resilience modulus of overlay (MPa)	Horizontal force coefficient	The maximum take-off weight of the designed aircraft (kN)
Actual value	18	1400	0.23	157.53
Conversion value (dimensionless)	86.8	60.4	43.9	52.9

when the impact of external environmental is not considered, the classification of working condition of Juba airport in South Sudan is 3.

The annual extreme minimum temperature of Juba airport is more than −9.0°C; the highest monthly mean temperature exceeds 30°C; the annual average rainfall is more than 1000 mm. Therefore, Juba Airport is located in climate II area. Table 9 shows that the comprehensive working conditions in Juba Airport in South Sudan can be classified as comprehensive classification II.

As shown in Table 16, it is recommended that Juba Airport should use geogrid + SBS-modified emulsified asphalt or ordinary hot asphalt as the interlayer treatment measures. However, only one runway is present in Juba Airport. To ensure the normal operation of airport, nonstop construction method should be used. Therefore, the use of modified emulsified asphalt is not allowed. Finally, the interlayer treatment measure is geogrid + ordinary hot asphalt.

6. Conclusions

(1) A mechanical model of asphalt concrete overlay of airport was established, and the variation trend of interlayer shear stress affected by different factors was obtained. The influencing trend of different factors on the interlayer shear stress of asphalt concrete overlay under B-767 aircraft load and BZZ-100 vehicle load was calculated and compared. The thickness of overlay has the greatest influence on the interlayer shear stress. The thickness increases from 5 cm to 20 cm, and the interlayer shear stress decreases by 45.5%.

(2) According to the analysis of mechanical response between overlays, the combined weight of each influencing factor was calculated using the AHP-entropy method. Combined with climate zoning in hot and humid areas, the working conditions of airport asphalt pavement overlay are divided into three levels. Comprehensive classification I is the worst; comprehensive classification III is the best.

(3) A new type of interlayer treatment measure is proposed: two oils and one aggregate, i.e., lower asphalt and intermediate crushed stones are first sprayed on the old pavement in sequence, and the top asphalt is covered on crushed stones, thus significantly improving the asphalt coverage of crushed stones, increasing the interlayer bonding between the old and new pavements, and effectively acting as a stress absorption layer. The optimum spraying amounts of three types of interlayer materials are combined with four types of interlayer treatment measures.

(4) Through indoor shear test, wheel-load fatigue test, and pressurized seepage test, the variation trends of shear, crack, and seepage performance of airport pavement overlay under different materials and treatment measures in humid and hot areas were obtained. With shear resistance as the main factor and crack resistance, impermeability, and rutting resistance as the supplementary factors, the best interlayer materials and treatment measures are SBS-modified asphalt and two oils and one material, respectively.

(5) Combined with the performance ranking of different materials and interlayer treatment measures, the recommended interlayer treatment measures for comprehensive classifications I, II, and III are two oils and one material + SBS-modified asphalt, asphalt precoating or geogrid + SBS-modified emulsified asphalt or ordinary hot asphalt, and geotextile + ordinary hot asphalt, respectively. Based on Juba airport, the working conditions are comprehensive classification II, and the recommended interlayer treatment measures are geogrid + ordinary hot asphalt.

Data Availability

The test data used to support the findings of this study have been deposited in the Hindawi (Journal of advanced transportation) repository. The test data are included within the article and can be made freely available.

Conflicts of Interest

The authors declare no conflicts of interest.

Acknowledgments

This research was funded by Construction of Science and Technology Projects by the Ministry of Communications of China (2018-MS2-042) Science and Technology Projects of Harbour Engineering Construction in China (SSD-SUB-KJYF-20150003), and Ministry of Transportation Science and Technology Demonstration Project (2017-04).

References

[1] L. W. Chen, J. M. Ling, J. Yuan, and M. Li, "Study on optimization model of the selection of distresses maintenance countermeasures for airport pavement," *Highway Engineering*, vol. 37, no. 3, pp. 79–84, 2012.

[2] J. M. Ling, Z. F. Zhou, and J. C. Peng, "Design and properties of storable asphalt mixture for rapid repair of airport pavement," *Journal of Building Materials*, vol. 10, no. 2, pp. 195–200, 2007.

[3] J.C. Y. Li, H. Chang, "Experimental study on interlayer mechanical behavior of airport composite pavement at turning area," *Journal of Highway and Transportation Research and Development*, vol. 36, no. 7, pp. 29–37, 2019.

[4] X. C. Yan, X. Z. Weng, and Y. N. Kou, "Influence of fiber grid on interlayer bond property of airport double-layer pavement," *Journal of Reinforced Plastics and Composites*, vol. 33, no. 1, pp. 101–111, 2017.

[5] X. C. Wang, Z. Y. Su, A. M. Xu, A. G. Zhou, and H. T. Zhang, "Shear fatigue between asphalt pavement layers and its application in design," *Construction and Building Materials*, vol. 135, pp. 297–305, 2017.

[6] S. Chun, K. Kim, J. Greene, and B. Choubane, "Evaluation of interlayer bonding condition on structural response characteristics of asphalt pavement using finite element analysis and full-scale field tests," *Construction and Building Materials*, vol. 96, pp. 307–318, 2015.

[7] H. Kim, M. Arraigada, C. Raab, and M. N. Partl, "Numerical and experimental analysis for the interlayer behavior of double-layered asphalt pavement specimens," *Journal of Materials in Civil Engineering*, vol. 23, no. 1, pp. 12–20, 2011.

[8] D. Zamora-Barraza and M. A. Calzada-Perez, D. Castro-Fresno and A. Vega-Zamanillo, "Evaluation of anti-reflective cracking systems using geosynthetics in the interlayer zone," *Geotextiles and Geomembranes*, vol. 29, no. 2, pp. 130–136, 2011.

[9] G. S. Cleveland, R. L. Lytton, and J. W. Button, "Using pseudostrain damage theory to characterize reinforcing benefits of geosynthetic materials in asphalt concrete overlays," *Transportation Research Record*, vol. 1849, pp. 202–211, 2003.

[10] G. Ferrotti, F. Canestrari, E. Pasquini, and A. Virgili, "Experimental evaluation of the influence of surface coating on fiberglass geogrid performance in asphalt pavements," *Geotextiles and Geomembranes*, vol. 34, pp. 11–18, 2012.

[11] N. Mai-Lan, J. Blanc, J. P. Kerzrého, and P. Hornych, "Review of glass fibre grid use for pavement reinforcement and APT experiments at IFSTTAR," *Road Materials and Pavement Design*, vol. 14, no. 1, pp. 287–308, 2013.

[12] E. Pasquini, M. Bocci, G. Ferrotti, and F. Canestrari, "Laboratory characterisation and field validation of geogrid-reinforced asphalt pavements," *Road Materials and Pavement Design*, vol. 14, no. 1, pp. 17–35, 2013.

[13] J.-S. Chen and C.-C. Huang, "Effect of surface characteristics on bonding properties of bituminous tack coat," *Transportation Research Record*, vol. 2180, pp. 142–149, 2010.

[14] B. Yu, Q. Lu, and J. Yang, "Evaluation of anti-reflective cracking measures by laboratory test," *International Journal of Pavement Engineering*, vol. 14, no. 6, pp. 553–560, 2013.

[15] Y. H. Fan, "Study on the interlayer treatment methods of old cement concrete pavement and asphalt overlay," *Highway Engineering*, vol. 40, no. 5, pp. 27–31, 2015.

[16] Y. W. Li, K. Mu, X. Shi, and X. C. Wang, "Impact of base-surface contact conditions on mechanical response of asphalt pavement," *Journal of Chang'an University (Natural Science Edition)*, vol. 34, no. 2, pp. 38–44, 2014.

[17] Z. G. Zhang, "Research on interlayer treatment technology of asphalt pavement," *Highway Transportation Technology (Applied Technology Edition)*, vol. 15, no. 3, pp. 62–64, 2019.

[18] X. Y. Jia and M. J. Zhang, "Study on the inter-layer connection of rubber asphalt gravel lower seal of asphalt pavement," *Northern Communications*, vol. 2, pp. 47–51, 2019.

[19] S.-Y. Zou, W.-C. Xi, M.-J. Peng, and Y.-M. Cheng, "Analysis of fracture problems of airport pavement by improved element-free Galerkin method," *Acta Physica Sinica*, vol. 66, no. 12, Article ID 120204, 2017.

[20] T. Li and A. A. Trani, "A least-square model to estimate historical percentages of itinerant general aviation operations by aircraft types and flight rules at an airport," *Journal of Advanced Transportation*, Article ID 9575676, 16 pages, 2017.

[21] Civil Aviation Administration of China, *MH/T 5010–2017 Specifications for Asphalt Pavement Design of Civil Airports*, China Civil Aviation Publishing House, Beijing, China, 2017.

[22] K. Cook, N. Garg, A. Singh, and M. Flynn, "Detection of delamination in the hma layer of runway pavement structure using asphalt strain gauges," *Journal of Transportation Engineering*, vol. 142, no. 11, Article ID 04016047, 2016.

[23] C. Y. Chan, B. S. Huang, X. D. Yan, and S. Richards, "Investigating effects of asphalt pavement conditions on traffic accidents in Tennessee based on the pavement management system (PMS)," *Journal of Advanced Transportation*, vol. 44, no. 3, pp. 150–161, 2010.

[24] Ministry of Communications of the People's Republic of China, *JTG D50–2017 Specifications for Design of Highway Asphalt Pavement*, China Communications Press, Beijing, China, 2017.

[25] K. Zhang, Z. Q. Zhang, and Y. F. Luo, "Material composition design and anticracking performance evaluation of asphalt rubber stress-absorbing membrane interlayer (AR-SAMI)," *Advances in Materials Science and Engineering*, Article ID 8560604, 11 pages, 2018.

[26] Ministry of Communications of the People's Republic of China, *JTG F40–2004 Technical Specifications for Construction of Highway Asphalt Pavements*, China Communications Press, Beijing, China, 2017.

[27] Ministry of Communications of the People's Republic of China, *JTG 5421-2018 Specifications for Maintenance Design of Highway Asphalt Payment*, China Communications Press, Beijing, China, 2018.

[28] Ministry of Communications of the People's Republic of China, *JTG E20 Standard Test Methods of Bitumen And Bituminous Mixtures for Highway Engineering*, China Communications Press, Beijing, China, 2011.

[29] H. W. Zhang, P. W. Hao, C. Tang, and Y. Pang, "Adherence of geotextile interlayer in asphalt overlay," *Journal of Building Materials*, vol. 20, no. 5, pp. 745–751, 2017.

[30] X. C. Wang, N. R. Fang, H. Y. Ye, and J. Zhao, "Fatigue damage analysis of cement-stabilized base under construction loading," *Applied Sciences-Basel*, vol. 8, no. 11, pp. 2263–2283, 2018.